Spin dynamics of Gd at high temperatures

J. W. Cable and R. M. Nicklow
Oak Ridge National Laboratory, Solid State Division, P.O. Box 2008, Oak Ridge, Tennessee 37831
(Received 31 October 1988)

The magnetic excitation spectra of Gd were measured by neutron inelastic scattering over the entire Brillouin zone in the ⟨110⟩ direction at temperatures from 250 to 850 K (T_c=293 K). The data were fitted to a damped-harmonic-oscillator form for the spectral weight function and were placed on an absolute cross-section basis. Wave-vector-dependent susceptibilities were obtained by integration over energy. They clearly show the presence of static spin correlations even at T=850 K. At $T \geq T_c$ we observe a crossover from spin-diffusive motion at small q to spin-wave behavior at large q. The wave vector q_c at which this crossover occurs is determined by the ratio of the damping parameter to the second moment, $\langle\omega^2\rangle$, of the frequency distribution. Surprisingly, $\langle\omega^2\rangle$ remains independent of temperature above T_c, and the temperature dependence of q_c is therefore determined by a gradual change in the damping. This results in a very weak q_c-versus-T dependence, which is not consistent with a magnetic short-range-order interpretation for the existence of spin waves above T_c.

INTRODUCTION

Much of the current interest in the spin fluctuations of ferromagnets at finite temperatures centers around the existence of propagating spin waves above T_c and the relationship between the presence of such excitations and the magnetic short-range order. Inelastic neutron scattering experiments have now been carried out for a variety of ferromagnets including the itinerant electron systems Fe and Ni,[1-3] the insulating Heisenberg system EuO (Refs. 4 and 5) and EuS,[6] and the metallic Heisenberg systems Gd,[7] Pd_2MnSn,[8,9] and Fe_3Si.[10]

Results for the itinerant electron systems remain controversial despite prodigious experimental efforts. The two principal research groups do not even agree on the experimental observations and offer conflicting interpretations for the spin-fluctuation behavior of these systems. The polarized neutron data of Mook and Lynn[2] on Ni at 1.06 T_c seem to show a crossover from spin-diffusion to spin-wave behavior near ζ=0.16 in the ⟨111⟩ direction. However, Shirane *et al.*[3] are unable to reproduce these results and prefer a spin-diffusion interpretation out to the highest q values for which measurements have been made, i.e., to a reduced wave vector of ζ=0.18 (q=0.56 Å^{-1}).

The experimental results for Pd_2MnSn (Refs. 8 and 9) and Fe_3Si (Ref. 10) have also been interpreted on the basis of a spin-diffusion model even out to large q. values. However, in neither case are the data good enough to discriminate against underdamped spin waves above T_c.

By contrast, the Heisenberg systems EuO,[4,5] EuS,[6] and Gd (Ref. 7) clearly exhibit a crossover from spin diffusion at small q to damped spin-wave behavior at large q." These results are completely in accord with current spin-fluctuation theories[11-13] which yield finite-frequency peaks for a disordered system whenever the second moment of the frequency distribution is somewhat larger than the square of the inverse relaxation time of the random forces.

In our previous neutron study[7] of the temperature dependence of the magnetic excitations in Gd, we found that the borderline between overdamped and underdamped spin fluctuations occurred at 1.09 T_c for zone-boundary spin waves in the ⟨00l⟩ direction. This was an unexpected result because underdamped spin waves apparently persist to 2 T_c in the similar Heisenberg systems EuO and EuS. We attributed this difference in behavior to the difference in the energetics of the spin systems relative to $k_B T_c$ and suggested that spin waves propagating along the more energetic ⟨110⟩ direction in Gd should persist to higher temperatures. In this paper we report neutron measurement for this harder ⟨110⟩ direction of Gd. Some of these results have been briefly described in a previous conference proceedings paper.[14]

EXPERIMENTAL PROCEDURE

The single crystal of ^{160}Gd is the same as that used in our previous study. It has a volume of about 3 cm^3 and a mosaic spread of about 20 ft. The sample was mounted with a ⟨100⟩ axis vertical, and data were obtained out to the zone boundary in the ⟨110⟩ direction around the reciprocal lattice points (002), (003), and (110). Data were taken at fixed temperatures of 250, 293, 320, 440, 586, and 850 K compared to the sample Curie temperature of T_c=293 K.

All measurements were made with the HB-2 triple-axis spectrometer at the High-Flux Isotope Reactor of the Oak Ridge National Laboratory. The data were taken at constant Q with fixed final energies of 3.60 and 3.32 THz and with a pyrolytic graphite filter in the scattered beam to remove higher-order contamination. Pyrolytic graphite was used for both the monochromator and the analyzer, and horizontal collimation of 40′ was used be-

fore and after the sample.

Typical results are shown in Figs. 1 and 2. The small-q behavior for a few selected temperatures is illustrated by Fig. 1 for $\mathbf{Q}=(0.1,0.1,2.0)$. Here, $\mathbf{Q}\equiv\mathbf{k}'-\mathbf{k}=\mathbf{G}\pm\mathbf{q}$ where $\mathbf{G}$ is a reciprocal lattice vector defined by $\mathbf{G}=2\pi(h_1\mathbf{b}_1+h_2\mathbf{b}_2+h_3\mathbf{b}_3)$. Thus, $\mathbf{Q}=(0.1, 0.1, 2.0)$ indicates a displacement by $\mathbf{q}+(0.1,0.1,0)$ from $\mathbf{G}=(0,0,2)$. At $T=250$ K (0.85 T_c) the data show a weak elastic peak and a strong spin-wave creation peak near 1.1 THz. With increasing temperature, the creation and annihilation peaks become broader and shift toward zero frequency until at $T=293$ K (1.0 T_c) the two peaks are no longer resolved and appear as a single Lorentzian-shaped peak centered at zero frequency. By contrast, the large-q data in Fig. 2 show a broad, but well-defined, spin-wave

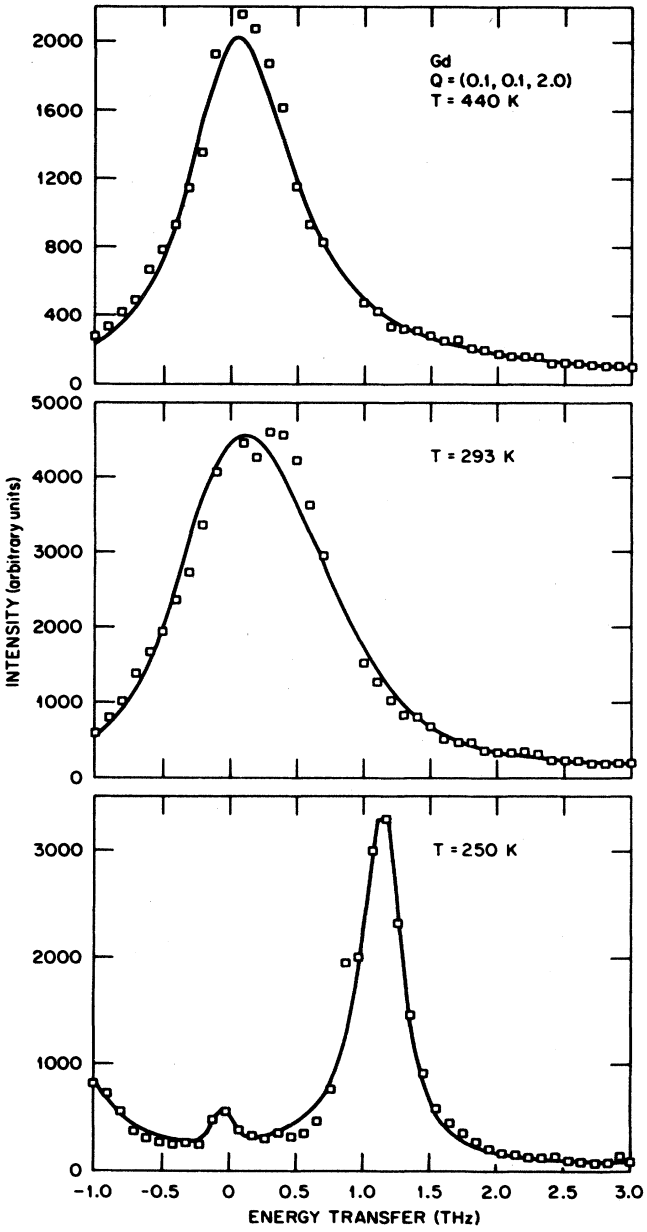

FIG. 1. Magnetic excitation spectra of Gd above and below T_c at $\mathbf{Q}=(0.1, 0.1,2.0)$. The solid curves are fitted to the data as described in the text. The high point at 0.9 THz in the 250 K spectrum corresponds to a TA phonon.

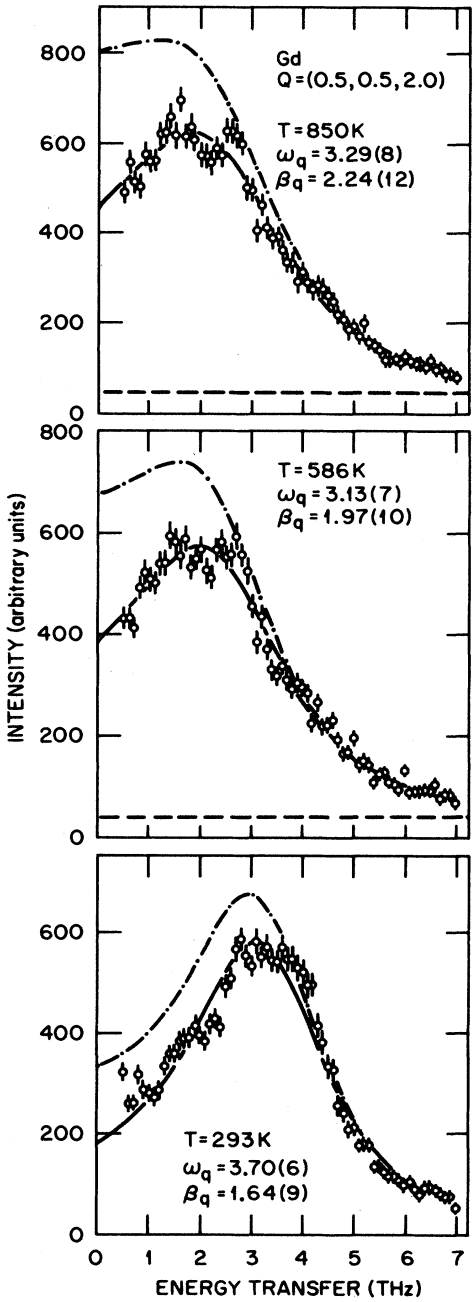

FIG. 2. Magnetic excitation spectra of Gd at $T\geq T_c$ and $\mathbf{Q}=(0.5,0.5,2.0)$. The solid curves are fitted to a DHO function and the dashed lines indicate the fitted-background levels (this is zero at $T=293$ K). The dashed-dot curves represent the fitted DHO curves after correction for $g(E)$, the higher-order-wavelength contamination in the monitor response (see text).

creation peak at $T=293$ K. With increasing temperature, this peak shifts slightly toward zero frequency but persists even to $T=850$ K (2.9 T_c). This is the theoretically expected behavior for Heisenberg ferromagnets above T_c. The long-wavelength spin fluctuations correspond to diffusive spin motion and this results in neutron scattering cross sections with Lorentzian frequency distributions centered on zero frequency for small q. The short-wave length fluctuations are collective spin oscillations which produce finite-frequency peaks at intermediate and large q.

ANALYSIS

The observed intensity distribution, $I(\mathbf{q},\omega)$, is proportional to the dynamic structure factor which can be written as

$$S(\mathbf{q},\omega)=(g\mu)^{-2}\omega(n_\omega+1)\chi_{\mathbf{q}}F(\mathbf{q},\omega)\ . \tag{1}$$

Here, $\hbar\omega$ is the energy transfer, n_ω is the Bose factor, $\chi_{\mathbf{q}}$ is the wave-vector-dependent susceptibility which describes the static spin correlations, and $F(\mathbf{q},\omega)$ is the spectral-weight function which defines the spin dynamics.

Theoretical expressions for the $F(\mathbf{q},\omega)$ of Heisenberg systems in the paramagnetic region have recently been obtained by Lindgård[12,13] who uses a Green's function approach with a mode-mode coupling approximation for the damping. He obtains a damped harmonic-oscillator (DHO) function for $F(\mathbf{q},\omega)$ which is quite convenient for the parametrization of data. In our previous study[7] of the magnetic excitations in Gd along the $\langle 00l\rangle$ direction, we found that our data were remarkably well described by this functional form over the entire Brillouin zone and for temperatures from 9 to 320 K. Because of this success and because the DHO function is expected to apply over a wide range of q, ω, and T, we have also fitted the present $\langle 110\rangle$ data with a DHO spectral weight function:

$$F(\mathbf{q},\omega)=\frac{1}{\pi}\frac{2\beta_q\langle\omega_q^2\rangle}{(\omega^2-\langle\omega_q^2\rangle)^2+4\beta_q^2\omega^2}\ . \tag{2}$$

Here, $\langle\omega_q^2\rangle$ is the second moment of the frequency distribution and β_q is a damping parameter related to the relaxation time of the random forces acting on the spins.

The solid curves in Figs. 1 and 2 are the result of a least-squares fit to the data with a constant background, a Gaussian elastic peak, and the DHO spectral-weight function convoluted with the instrumental resolution function. Here, the DHO function was first multiplied by the detailed balance factor and by a function $g(E)$ which is the fraction of the monitor counts due to neutrons with incident energy E. This function was experimentally determined by integrated-intensity measurements of the higher-order Bragg peaks from polycrystalline silicon and diamond. We note that this entire data set has unusually good statistical accuracy because of the large size and low-neutron absorption of the ^{160}Gd sample and because of the high-spin value ($S=\frac{7}{2}$) of Gd. Good tests of the functional form for $F(q,\omega)$ are therefore to be expected. The DHO provides an excellent description for the zone-boundary spectra in Fig. 2. The fits are not quite so good for the small-q spectra at $T\geq T_c$ in Fig. 1 where a single Lorentzian spectral-weight function might be more appropriate. However, in this regime where the damping becomes very large, the DHO function assumes an approximately Lorentzian form with an inverse relaxation time given by $\Gamma_q=\langle\omega_q^2\rangle/2\beta_q$. We have therefore parameterized the entire data set with the DHO function, and the fitted parameters are listed in Tables I and II. Here, I_0 is the intensity in units of counts monitor^{-1} THz^{-1}, and the characteristic frequency, ω_q, has been defined as

$$\omega_q\equiv\langle\omega_q^2\rangle^{1/2}\ . \tag{3}$$

The actual peak position in the frequency distribution is not ω_q but, instead, is given by

$$\omega_{\text{peak}}^2=\langle\omega_q^2\rangle-2\beta_q^2\ . \tag{4}$$

TABLE I. Magnetic parameters for Gd.

($E'=3.6$ THz, $C=19.7$ cts/b)

T(K)	$\zeta(4\pi/a)$	I_0(THz^{-1})	ω_q (THz)	β_q (THz)
		$\mathbf{Q}=(\zeta,\zeta,2)$		
293	0.1	9.1	0.76(4)	0.61(8)
	0.2	4.9(2)	2.07(4)	0.99(6)
	0.3	4.5(2)	3.00(4)	1.52(6)
	0.4	3.6(2)	3.48(4)	1.60(6)
	0.5	3.0(2)	3.67(6)	1.66(10)
440	0.1	5.2	1.2	2.0
	0.2	3.5(2)	1.80(4)	1.19(8)
	0.3	2.9(2)	2.48(4)	1.45(6)
	0.35	2.7(2)	2.80(7)	1.67(11)
	0.4	2.5(1)	2.94(5)	1.74(8)
	0.45	2.3(2)	3.09(7)	1.78(10)
	0.5	2.2(2)	3.23(4)	1.97(7)
586	0.1	3.3	1.3	2.2
	0.2	2.6(2)	1.98(7)	1.59(14)
	0.3	2.3(2)	2.47(5)	1.58(9)
	0.4	2.0(1)	2.90(6)	1.80(10)
	0.5	1.7(1)	3.18(7)	2.08(10)
850	0.1	2.2	1.5	2.2
	0.2	1.7(2)	1.93(10)	1.67(21)
	0.3	1.6(2)	2.58(8)	1.80(14)
	0.35	1.5(1)	2.83(9)	1.88(13)
	0.4	1.4(1)	3.03(8)	1.97(12)
	0.45	1.3(1)	3.16(10)	2.14(16)
	0.5	1.3(1)	3.32(8)	2.31(12)
		$\mathbf{Q}=(1-\zeta,1-\zeta,0)$		
293	0.1	9.0	1.39	1.59
	0.2	4.7(3)	2.25(4)	1.35(6)
	0.3	4.6(2)	2.90(4)	1.67(7)
	0.4	4.1(3)	3.27(6)	2.03(10)
	0.5	5.4(4)	4.46(8)	3.54(13)
440	0.35	3.1(2)	2.39(4)	1.55(8)
	0.4	2.8(2)	2.46(5)	1.46(8)
	0.45	2.6(2)	2.47(6)	1.62(10)
	0.5	2.9(3)	2.81(11)	2.19(18)

The q dependence of the ω_q and β_q parameters is shown in Figs. 3 and 4. The $T \leq T_c$ results are given in Fig. 3 and show parameters that are strongly dependent on both q and T. At $T=250$ K, the β_q remain small over the entire zone, and the ω_q attain approximately 85% of their low-temperature values. With increasing temperature, the ω_q decrease and the β_q increase until at $T=293$ K, $\omega_q \sim \beta_q$ at our smallest q values. The $T > T_c$ results given in Fig. 4 show that the damping parameters β_q continue to increase with temperature but reveal an interesting saturation effect for the ω_q which become essentially temperature independent above T_c.

This effect is perhaps better illustrated by Fig. 5 which shows the temperature dependence of the ω_q and β_q parameters for fixed q values. Here, the ω_q and β_q are strongly temperature dependent only below and near T_c. Above T_c the ω_q appear temperature independent while the β_q increase slowly with temperature Note that this applies not only at the zone boundary $\mathbf{Q}=(0.5,0.5,2.0)$ but also at intermediate $\mathbf{Q}$. The temperature dependence of ω_{peak}, as calculated from Eq. (4), is also shown in Fig. 5. A finite-frequency peak remains at the zone boundary even at $T=850$ K ($2.9T_c$), while at $Q=(0.2,0.2,2.0)$, the frequency distribution has collapsed to a zero-frequency peak near $T=586$ K ($2.0\ T_c$).

According to Eq. (4), this crossover from a distribution with peaks at finite frequencies to a single peak at zero frequency occurs when $\beta_q = 0.707\ \omega_q$. The wave vector at which this occurs for a given temperature can therefore be determined from the q dependence of the ratio β_q/ω_q. This is shown in Fig. 6 where the horizontal dashed line represents the crossover boundary, and the intersection of this boundary with the solid curves defines the crossover wave vector, ζ_c. The T dependence of ζ_c is given in the insert; this shows a gradual increase of ζ_c with temperature for $T \geq T_c$. Diffusive-type spin fluctuations occur in the q-T region below the solid curve while spin-wave-like fluctuations appear above.

The q dependence of ω_{peak} is shown in Fig. 7. Here, the dashed lines are extrapolations of the $T \geq T_c$ data to the ζ_c values determined from Fig. 6. Notice that dispersion, which indicates the presence of collective spin fluctuations, persists to high temperatures.

TABLE II. Magnetic parameters for Gd.

($E'=3.32$ THz, $C=8.9$ counts/b)

$T(K)$	$\zeta(4\pi/a)$	I_0 (THz^{-1})	ω_q(THz)	β_q(THz)
		$\mathbf{Q}=(\zeta,\zeta,2)$		
250	0.1	4.01(17)	1.22(1)	0.18(1)
	0.2	1.59(6)	2.80(2)	0.34(2)
	0.3	0.87(5)	3.84(2)	0.33(3)
	0.4	0.65(5)	4.98(3)	0.34(5)
	0.5	0.47(5)	4.87(3)	0.27(6)
293	0.1	4.17(45)	0.91(4)	0.66(5)
	0.2	2.27(23)	2.23(7)	1.24(10)
	0.3	1.96(20)	3.05(8)	1.73(12)
	0.4	1.61(15)	3.53(9)	2.05(14)
	0.5	1.43(21)	3.75(12)	2.11(19)
320	0.1	3.62(48)	0.88(5)	0.93(10)
	0.2	2.08(21)	2.02(7)	1.27(10)
	0.3	1.70(10)	2.69(5)	1.51(8)
	0.4	1.45(10)	3.06(6)	1.72(10)
	0.5	1.21(8)	3.20(6)	1.72(10)
		$\mathbf{Q}=(\zeta,\zeta,3)$		
250	0.0	0.97(8)	2.93(2)	0.36(5)
	0.1	0.82(6)	3.36(3)	0.41(4)
	0.2	0.68(5)	4.07(3)	0.49(5)
	0.3	0.56(5)	4.21(4)	0.49(6)
	0.4	0.55(4)	3.47(3)	0.37(5)
	0.5	0.65(7)	3.00(3)	0.35(6)
293	0.0	1.51(22)	2.51(10)	1.53(16)
	0.1	1.56(26)	2.77(14)	1.85(22)
	0.2	1.40(23)	3.20(13)	1.81(20)
	0.3	1.29(27)	3.26(18)	1.97(26)
	0.4	1.11(21)	2.57(12)	1.28(17)
	0.5	1.25(21)	2.60(12)	1.49(18)
320	0.0	1.38(23)	2.24(12)	1.57(20)
	0.1	1.43(20)	2.56(12)	1.91(20)
	0.2	1.49(31)	3.29(20)	2.36(30)
	0.3	1.23(15)	2.97(10)	1.78(15)
	0.4	1.31(25)	2.71(16)	1.86(24)
	0.5	1.28(24)	2.56(18)	1.91(30)

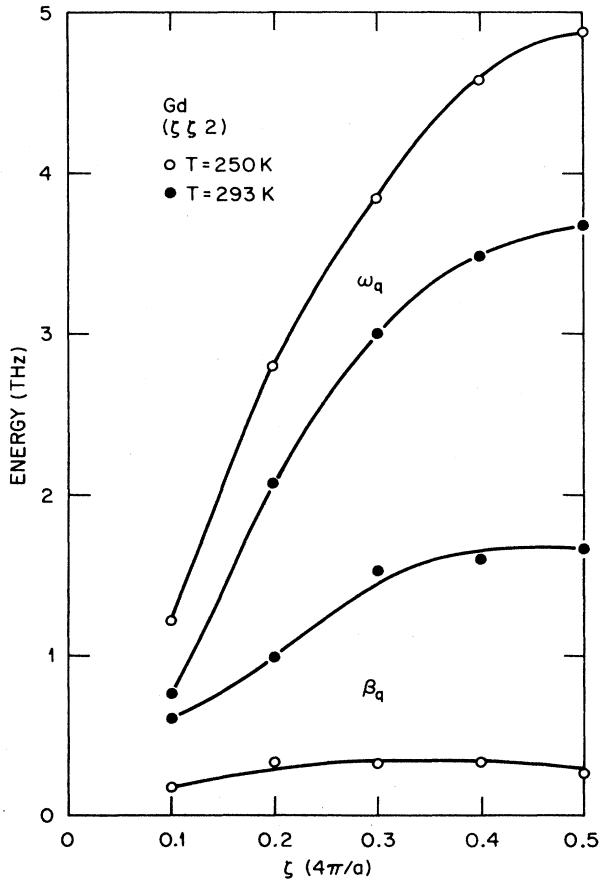

FIG. 3. Wave vector dependence of the ω_q and β_q parameters for $T \leq T_c$. ($\omega_q \equiv \langle \omega_q^2 \rangle^{1/2}$).

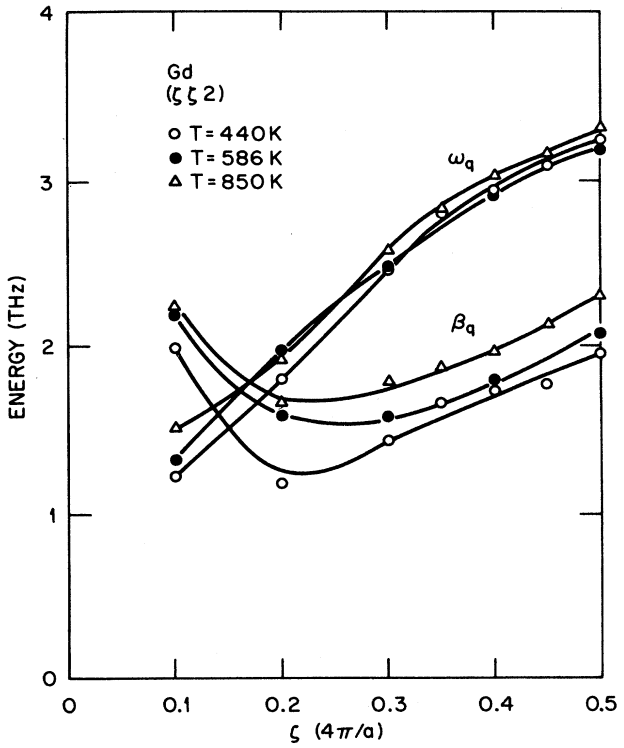

FIG. 4. Wave-vector dependence of ω_q and β_q for $T > T_c$.

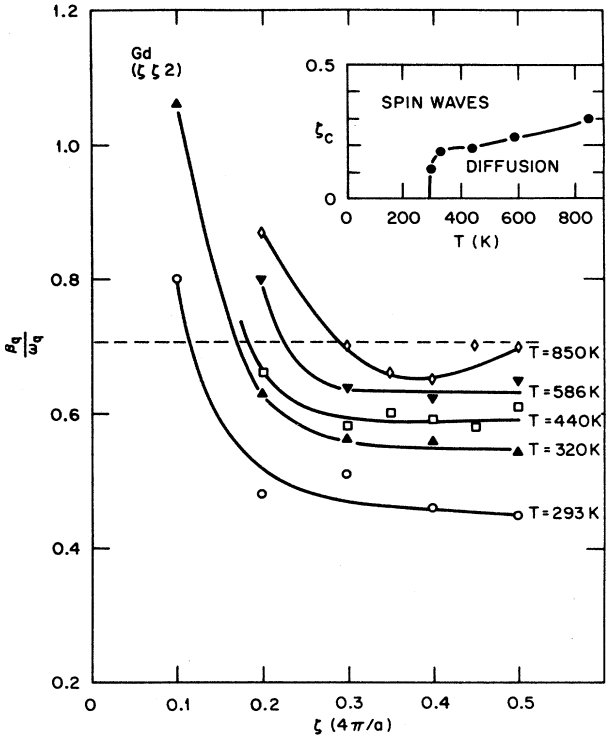

FIG. 6. Wave vector dependence of β_q/ω_q at fixed T. The horizontal dashed line is the crossover boundary between diffusive (above) and spin-wave (below) behavior. The inset shows the T dependence of the crossover wave vector, ζ_c.

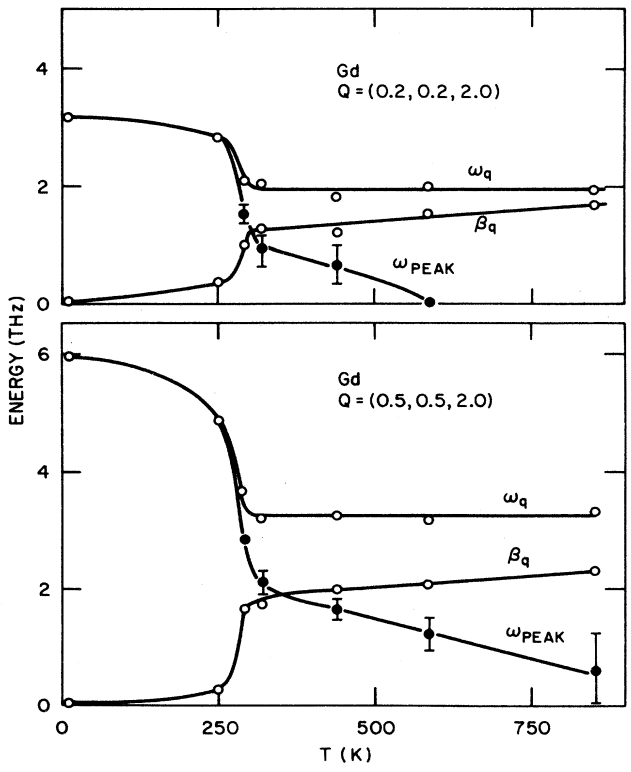

FIG. 5. Temperature dependence of ω_q, β_q, and ω_{peak} at fixed Q. ω_{peak} is calculated from the fitted parameters by use of Eq. (4).

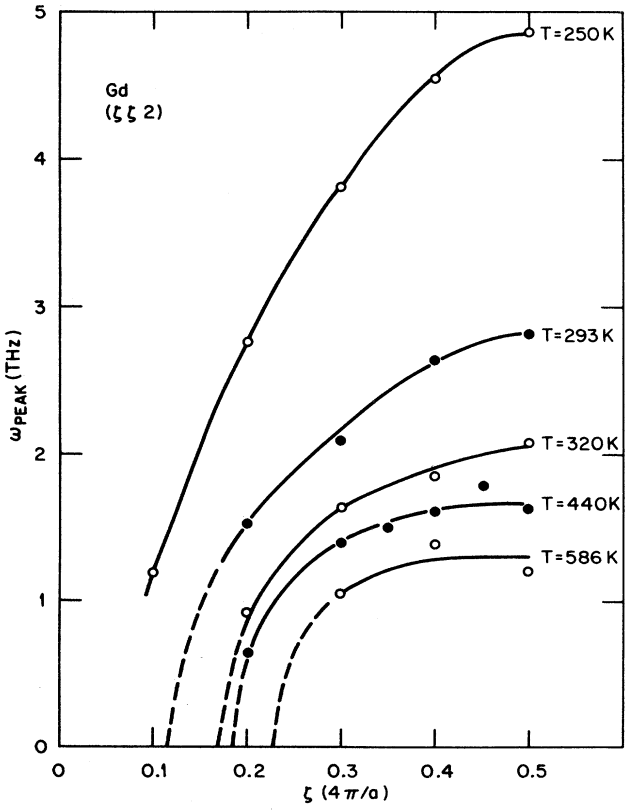

FIG. 7. Wave-vector dependence of ω_{peak}. The dashed curves are extrapolated to the ζ_c from Fig. 6.

THE OPTIC BRANCH

The hcp structure of Gd can be described in terms of two interpenetrating Bravais sublattices with inter- and intra-sublattice interactions J_R and J_R'. There are then two spin-wave branches which, for long wavelength modes, correspond to in-phase and anti-phase precession of the spins in the two sublattices. These are referred to as acoustic and optic spin waves, respectively. A few measurements were made on the optic spin fluctuations at $\mathbf{Q}=(\zeta,\zeta,3)$, and the fitted parameters for these data are listed in Table II. Here again, the $T=250$ K data yield β_q parameters that are small over the entire zone while the ω_q parameters attain about 85% of their low-temperature values. At 293 K, the ω_q values have decreased by only about 20%, but the damping parameters have increased significantly. Nevertheless, the β_q/ω_q ratios lie well below the crossover boundary for the entire zone so that finite-frequency peaks occur at all q for the optic branch at T_c. Above T_c at $T=320$ K, the β_q/ω_q ratios lie quite near the crossover boundary for the entire zone except for the $\zeta=0.3$ data near the K point in the zone.

The q dependences of the ω_q and β_q parameters for both the acoustic and optic branches at $T=293$ K and 320 K are shown in Fig. 8. The degeneracy in ω_q previouly observed[15] at the K point for low temperatures apparently persists to $T\geq T_c$. It is interesting that the β_q parameters exhibit the same type of crossing pattern and degeneracy at the K point at 293 K, and that similar tendencies persist even above T_c at 320 K. This results from completely different damping behavior of the acoustic and optic spin fluctuations. The damping of the optic, or antiphase, spin fluctuations is nearly independent of q while the acoustic damping is weak at small q but increases with q in such a way that the β_q parameters for the two branches are nearly the same at the K point. We have already seen that finite-frequency peaks persist at $T\geq T_c$ for the acoustic spin fluctuations even at modest q values. It is not surprising then, that a finite-frequency peak remains at $T=320$ K for the optic branch at $\zeta=0.3$ where both the frequency distribution and the damping are nearly the same for the two branches.

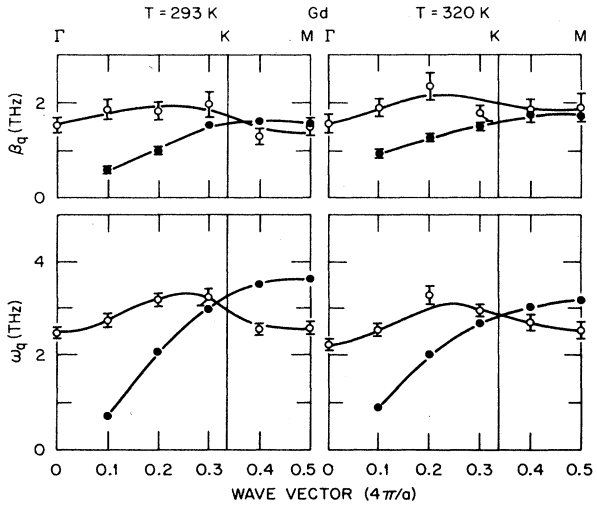

FIG. 8. Wave vector dependence of ω_q and β_q for the acoustic (closed circles) and optic (open circles) spin fluctuations at $T=293$ and 320 K.

THE SCATTERING LAW

The spectra shown in Figs. 1 and 2 are raw intensity data which include the instrumental background, an elastic peak from various scattering sources, and phonon scattering from the sample. In addition, the frequency distributions are distorted due to the detailed balance factor and because of an energy-dependent monitor response derived from higher-order wavelength contamination in the incident beam. Because of these distorting features, the thermal evolution of the spin fluctuations is better described by the observed behavior of the fitted parameters, as in Figs. 3–6, or by the evolution of the actual scattering law as calculated from these parameters. We note that these distorting features have little effect on the fitted parameters. The background is quite low and is included as a fitting parameter. Insignificant changes in the parameters were found when spectra were fitted with and without inclusion of the elastic and/or phonon peaks. Furthermore, the detailed balance factor is a known function of $\hbar\omega/k_BT$ and the uncertainty in our experimentally determined $g(E)$ function introduces an error of less than 1% in the fitted parameters. The uncertainties in these parameters are well represented by the statistical errors indicated in Tables I and II. Three-dimensional projections of the actual scattering law are displayed in Fig. 9. Here the scattering law is defined by $I_0F(q,\omega)/Cf^2(\mathbf{Q})$ [see Eq. (5)] and is in absolute units of b THz^{-1}. For scaling reasons, these have been truncated in the small-q, high-intensity regions. Even so, they show clearly the evolution of the frequency distributions with temperature. In particular, the projections for the three highest temperatures show that increasing q values are required for the occurrence of finite-frequency peaks. For example, the finite-frequency peak at $\zeta=0.3$ and $T=440$ K is less pronounced but still discernable at $T=586$ K and apparently no longer present at $T=850$ K. These are the same general conclusions as were obtained from the ω_q and β_q parameter behavior, but these scattering-law projections provide a more immediate physical picture of the magnetic response.

THE SUSCEPTIBILITY

The intensity per monitor count is given by[16]

$$\frac{I(\mathbf{q},\omega)}{g(E)}=C\left[\frac{e^2\gamma}{mc^2}\right]^2 f^2(\mathbf{Q})\frac{k'}{k}S(\mathbf{q},\omega)\ , \tag{5}$$

where $g(E)$ is the fraction of the monitor counts due to neutrons with incident energy E, C is the calibration constant, $f(\mathbf{Q})$ is the magnetic form factor, and k and k' are the incident and scattered wave vectors. $S(\mathbf{q},\omega)$ can be written as

$$S(\mathbf{q},\omega)=\sum_{\alpha}(1-\hat{Q}_{\alpha}^{2})S^{\alpha}(\mathbf{q},\omega)\ , \tag{6}$$

where α denotes a Cartesian component and $\hat{Q}_{\alpha}$ is the α-direction cosine of $\mathbf{Q}$. The generalized wave vector dependent susceptibility is obtained by integration of Eq. (5) over energy. This yields

$$I_0=C\left[\frac{e^2\gamma}{mc^2}\right]^2 f^2(\mathbf{Q})\frac{\chi_q}{g^2\mu^2}\ , \tag{7}$$

where I_0 is the intensity fitting parameter in Tables I and II and χ_q is given by

$$\chi_q=\sum_{\alpha}(1-\hat{Q}_{\alpha}^{2})\chi_q^{\alpha}\ . \tag{8}$$

Thus, χ_q is readily determined if the calibration constant is known.

In our earlier study[7] of the magnetic excitations in Gd, the data were internally calibrated by the energy integration of the low-temperature spin-wave intensities. The present data are calibrated by direct comparison with those previous data for a few scans at the same $\mathbf{Q}$ and T. Thus, the I_0 parameters shown in Table II for $\mathbf{Q}=(0,0,3)$ at three different temperatures were compared with the previous data to obtain the calibration constant of $C=8.9$ counts monitor^{-1} b^{-1} which is applicable to all of the data in Table II. Intercomparison of the $\mathbf{Q}=(\zeta,\zeta,2)$ data at $T=293$ K in Tables I and II was then used to obtain $C=19.7$ counts monitor^{-1} b^{-1} for the data of Table I.

In Lindgård's correlation theory,[13] the transverse susceptiblity, defined as $\chi_q^{\perp}\equiv\chi_q^{x}+\chi_q^{y}$, is given by

$$\chi_{q\perp}^{\pm}=\frac{2g^2\mu^2}{J_0^{\pm}R_q^{\pm}-J_q^{\pm}}\ , \tag{9}$$

where the $\pm$ sign refers to acoustic and optic spin fluctuations, respectively. Here,

$$J_q^{\pm}\equiv J_q\pm|J_q'|\ , \tag{10}$$

where J_q and J_q' are Fourier transforms of the inter- and intra-sublattice exchange interactions and $J_0^{+}R_q^{\pm}$ corresponds to an inverse cluster susceptibility. The first frequency moment is inversely related to the transverse susceptibility and is given by

$$\langle\omega_q^{\pm}\rangle=\langle S^z\rangle(J_0^{+}R_q^{\pm}-J_q^{\pm})\ . \tag{11}$$

At low temperatures, where the damping is small and the correlation effects are negligible, $R_q^{\pm}$ approaches unity and Eq. (11) reduces to the linear-spin-wave form for which $\langle\omega_q\rangle$ is proportional to $\langle S^z\rangle$. However, $R_c^{\pm}$ increases with temperature as the correlations become important. The spin-wave energies are shifted upward and are no longer directly proportional to $\langle S^z\rangle$. This effect was observed in our previous study of Gd and is illustrated here by Fig. 10 which shows the χ_q as calculated from

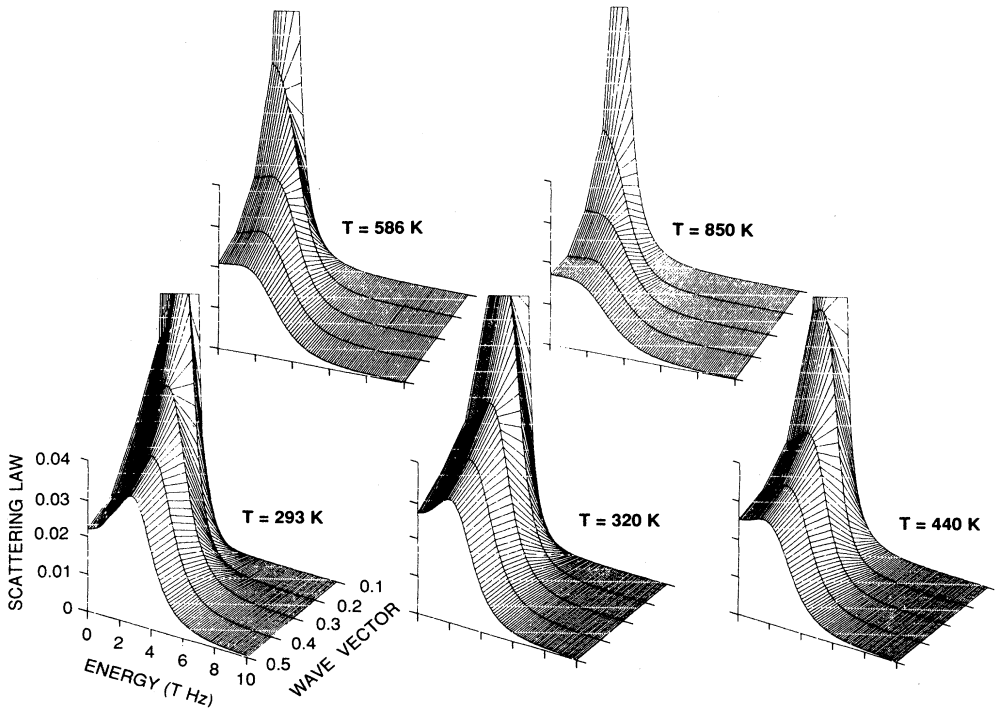

FIG. 9. Three-dimensional projections of the scattering law at $T\geq T_c$. All five projections have the same scales as those shown for the $T=293$ K projection. The scattering-law scale is given by $I_0F(\mathbf{q},\omega)/Cf^2(\mathbf{Q})$ and is in absolute units of b THz^{-1}.

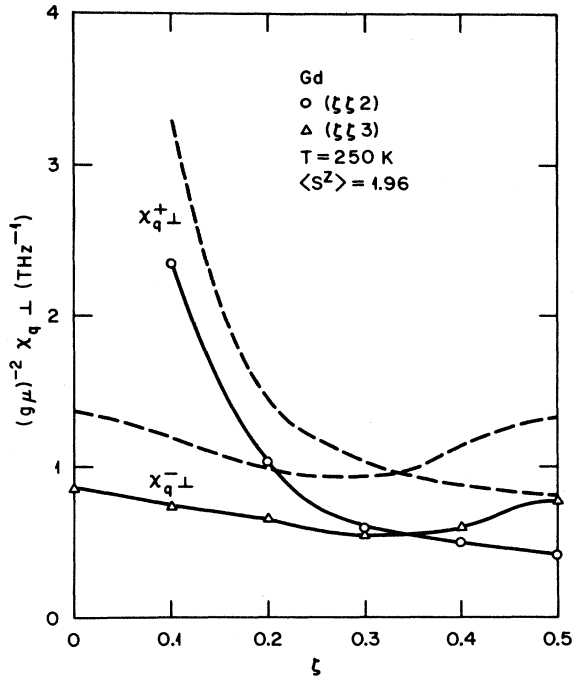

FIG. 10. Comparison of the observed magnetic susceptibilities with those calculated from spin-wave theory. The data points are the acoustic (+) and optic (−) susceptibilities as calculated from Eq. (7) while the dashed curves are from spin-wave theory, i.e., $\chi_{q\perp}^{\pm}=2\langle S^z\rangle/\omega_q^{\pm}$.

Eq. (7) for both the acoustic and optic modes at $T=250$ K. Here, we assume $\chi_q^x=\chi_q^y$ and $\chi_q^z=0$ where the z axis is defined by the direction of the ordered moment. (For Gd at $T=250$ K, z is parallel to the c-axis.) The calculated values of $\chi_{q\perp}^{\pm}/g^2\mu^2$ are shown as the data points while the dashed curves represent $2\langle S^z\rangle/\omega_q^{\pm}$ with $\langle S^z\rangle=1.96$ taken from bulk magnetization measurements[17] and with the $\omega_q^{\pm}$ taken from Table II. Clearly, the χ_q functions obtained by energy integration of $S(\mathbf{q},\omega)$ and by taking the inverse spin-wave energies have the same shape but not the same magnitude. This shows that $\omega_q^{\pm}$ is no longer directly proportional to $\langle S^z\rangle$ at this elevated temperature. This is also apparent from a direct comparison of the $\omega_q(T)$ and the bulk magnetization, $\sigma(T)$, where we find $\omega_q(T=250\text{ K})/\omega_q(T=10\text{ K})\simeq 0.85$ while $\sigma(250)/\sigma_0\sim 0.56$.

As T approaches T_c from below, the longitudinal susceptbility, χ_q^z, becomes finite and should diverge at $T=T_c$ and $q=0$. In an isotropic system, all three susceptibility components are equal for $T\geq T_c$. However, although Gd has an isotropic exchange interaction, it also has a uniaxial crystal structure so that the condition $\chi_q^x=\chi_q^y\neq\chi_q^z$ may well apply. In that event, χ_q must be written as in Eq. (8) without a separation into transverse and parallel susceptibilities. We can examine this inequality condition by comparison of data taken along $\mathbf{Q}=(\zeta,\zeta,2)$ and $\mathbf{Q}=(1-\zeta,1-\zeta,0)$. These different $\mathbf{Q}$ directions offer a partial separation because $\hat{\mathbf{Q}}_z^2\simeq 1$ for the $(\zeta\zeta 2)$ data, while $\hat{\mathbf{Q}}_z^2=0$ for the $(1-\zeta,1-\zeta,0)$ data. The respective susceptibilities are then $\chi_q\simeq 2\chi_q^x$ and $\chi_q=\chi_q^x+\chi_q^z$. Here, z is taken parallel to the c axis. This comparison of χ_q for the two $\mathbf{Q}$ directions is given in Fig. 11. There may be a difference in the χ_q for the two directions at $\zeta=0.1$, but unfortunately, this is the region where Lorentzian-shaped peaks developed at $T\geq T_c$ and the region for which the DHO-fitted parameters have the largest uncertainty. However, there is no significant difference in the χ_q over the rest of the Brillouin zone, and here we must conclude that $\chi_q^x=\chi_q^y=\chi_q^z$ even for this uniaxial system. The observed χ_q can therefore be written as $\chi_q=2\chi_q^x=\chi_{q\perp}$ for all of the present data at $T\geq T_c$. The corresponding $\chi_{q\perp}$ for the acoustic spin fluctuations are shown in Fig. 12. Formally χ_q is the Fourier transform of a spin-pair correlation,[16]

$$\chi_q^x=\frac{g^2\mu^2}{k_BT}\sum_{\mathbf{R}}e^{i\mathbf{q}\cdot\mathbf{R}}\langle S_0^xS_R^x\rangle\ . \tag{12}$$

At small q this assumes the Ornstein-Zernike form, $\chi_q=\chi_c/r_1^2(\kappa_1^2+q^2)$, where κ_1 is the inverse spin correlation length. This correlation length is quite large at $T=T_c$ where χ_q peaks sharply at $q=0$, but κ_1 increases with increasing $T-T_c$ and the $q=0$ peak becomes less pronounced. Finally, as $T\to\infty$, only the $R=0$ correlations remain, and χ_q becomes q independent. This general behavior is clearly present in Fig. 12 which shows data over the temperature range from $T=T_c$ to $T=2.9$ T_c. Even at the highest temperature, there is a peaking at small q indicative of remaining spin-pair correlations.

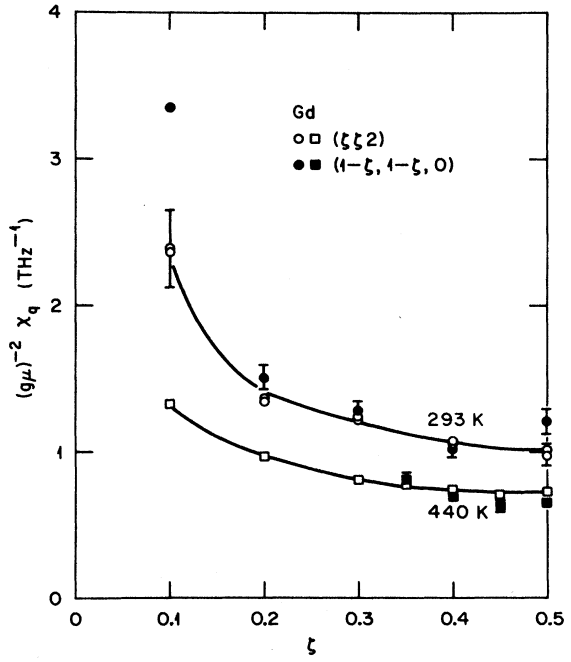

FIG. 11. Comparison of χ_q^+ for the two directions $\mathbf{Q}=(\zeta,\zeta,2)$ and $\mathbf{Q}=(1-\zeta,1-\zeta,0)$ at $T\geq T_c$. The corresponding susceptibilities are $\chi_q\simeq 2\chi_q^x$ and $\chi_q=\chi_q^x+\chi_q^z$, respectively.

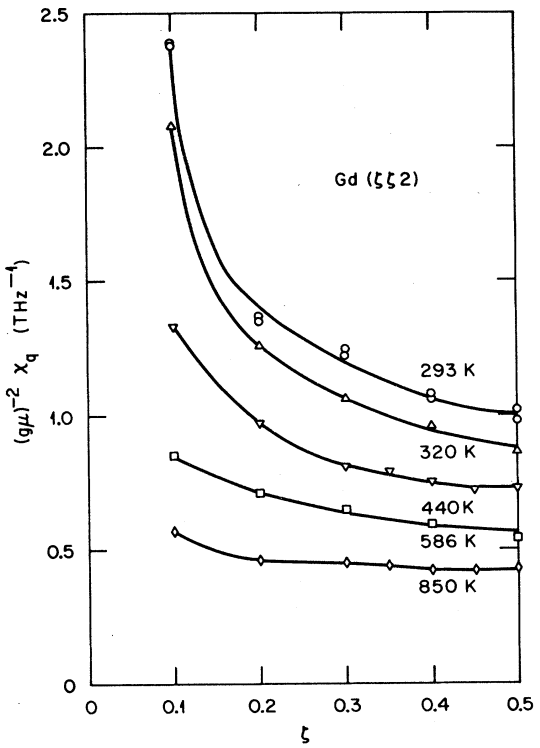

FIG. 12. $\chi_{q\perp}^{+}$ for Gd at $T \geq T_c$.

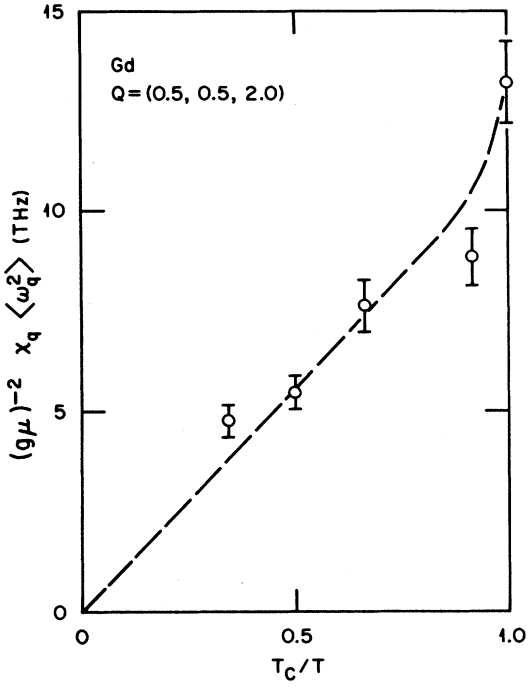

FIG. 13. Temperature dependence of $\chi_q\langle\omega_q^2\rangle$ at the zone boundary.

DISCUSSION

The existence of spin waves above T_c has often been associated with the presence of magnetically short-range-ordered regions with sufficiently large correlation lengths to support short-wavelength spin waves. In principle, this can be tested by comparing the temperature dependence of the crossover wavevector, ζ_c with that of the inverse correlation length, κ_1. Unfortunately, the present χ_q results do not extend into the small-q region required to extract κ_1 values. Furthermore, the earlier measurements by Child[18] extend only to about 1.2 T_c. Thus, we can only compare with the temperature dependence $\kappa_1 \sim (T-T_c)^{0.7}$ as calculated[19] by various expansion methods. The temperature dependence of ζ_c is shown in the inset of Fig. 6 and is much weaker than this *calculated* κ_1-versus-T dependence. This suggests that the spin waves observed in Gd at $T \geq T_c$ are not associated with the presence of magnetic short-range order. There is, however, a clear need for κ_1 measurements at temperatures higher than those presently available.

One of the most interesting results of this study is the temperature dependence of ω_q, β_q, and ω_{peak}, as illustrated by Fig. 5. This figure clearly shows that $\omega_q \equiv \langle\omega_q^2\rangle^{1/2}$ is independent of temperature in the range from T_c to nearly 3 T_c. The second frequency moment is a complicated function given by[16]

$$\langle\omega_q^2\rangle = \frac{4g^2\mu^2}{\chi_q^x}\sum_{\mathbf{R}} J_R(1-e^{i\mathbf{q}\cdot\mathbf{R}})\langle S_0^z S_R^z\rangle \tag{13}$$

for which temperature-dependent spin-pair correlations appear in both the numerator and denominator. Furthermore, the J_R for Gd remain finite out to several neighbor shells, so $\langle\omega_q^2\rangle$-versus-T is not readily calculable. However, the expression can be evaluated in the high-temperature limit where[16]

$$\langle\omega_q^2\rangle = \tfrac{8}{3}S(S+1)\sum_{\mathbf{R}} J_R^2(1-e^{i\mathbf{q}\cdot\mathbf{R}}) . \tag{14}$$

With J_R values taken from Lindgård,[20] this sum yields $\langle\omega_q^2\rangle = 1.07$ THz^2 at the $\langle 110\rangle$ zone boundary compared to our observed value of $\langle\omega_q^2\rangle \simeq 10$ THz.^{2}. This discrepancy suggests that $\langle\omega_q^2\rangle$ must eventually decrease with increasing T, and that the spin-pair correlations are still important even at 850 K. This is perhaps better illustrated by Fig. 13 which shows zone-boundary values of $(g\mu)^{-2}\chi_q\langle\omega_q^2\rangle$ versus the inverse temperature, T_c/T. In the limit as $T_c/T \to 0$, $\chi_q\langle\omega_q^2\rangle$ must approach zero. The fact that the 850 K data point is far from that limit shows that spin-pair correlations still extend beyond $R=0$ at 850 K.

Finally, we reiterate that finite-frequency peaks occur over a large part of the Brillouin zone in the $\langle 110\rangle$ direction for Gd at $T \geq T_c$. With increasing $(T-T_c)$, these peaks shift down in frequency and eventually collapse onto zero frequency, but the collapse occurs only because of a gradually increasing amount of damping. In Gd then, it is not the thermal breakup of spin-pair correlations but rather an increase in the mode-mode coupling that destroys the spin waves for $T > T_c$. In our earlier neutron study[7] of Gd, we suggested that spin waves prop-

agating along the more energetic ⟨110⟩ direction should persist to higher $(T-T_c)$ than those in the ⟨001⟩ direction. The present result confirms that expectation but also reveals that our intuition was better than our insight since the determining factor for spin waves above T_c appears to be the damping and not the second frequency moment. The relationship between the temperature dependence of the damping and the energetics of the spin system is not at all obvious.

ACKNOWLEDGEMENTS

The authors are indebted to T. L. Collins and J. R. Weir for technical assistance and to J. F. Cooke, P. Lindgård, S. H. Liu, and S. W. Lovesey for enlightening discussions of various aspects of this problem. This research was supported by the Division of Materials Sciences, U. S. Department of Energy under Contract No. DE-AC05-84OR21400 with Martin Marietta Energy Systems, Inc.

[1]H. A. Mook and J. W. Lynn, J. Appl. Phys. **57**, 3006 (1985).
[2]H. A. Mook and J. W. Lynn, Phys. Rev. Lett. **57**, 150 (1986).
[3]G. Shirane, P. Böni, and J. L. Martinez, Phys. Rev. B **36**, 881 (1987).
[4]H. A. Mook, Phys. Rev. Lett. **46**, 508 (1981).
[5]P. Böni and G. Shirane, Phys. Rev. B **33**, 3012 (1986).
[6]H. G. Bohn, A. Kollmar, and W. Zinn, Phys. Rev. B **30**, 6504 (1984).
[7]J. W. Cable, R. M. Nicklow, and N. Wakabayashi, Phys. Rev. B **32**, 1710 (1985).
[8]G. Shirane, Y. J. Uemura, J. P. Wicksted, Y. Endoh, and Y. Ishikawa, Phys. Rev. B **31**, 1227 (1985).
[9]M. Kohgi, Y. Endoh, Y. Ishikawa, H. Yoshizawa, and G. Shirane, Phys. Rev. B **34**, 1762 (1986).
[10]L. Pintschovius, Phys. Rev. B **35**, 5175 (1987).
[11]S. W. Lovesey and R. A. Meserve, J. Phys. C **6**, 79 (1973).
[12]P. Lindgård, Phys. Rev. B **27**, 2980 (1983).
[13]P. Lindgård, J. Magn. Magn. Mater. **54-57**, 981 (1986).
[14]J. W. Cable, R. M. Nicklow, and N. Wakabayashi, J. Magn. Magn. Mater. **54–57**, 1173 (1986).
[15]W. C. Koehler, H. R. Child, R. M. Nicklow, H. G. Smith, R. M. Moon, and J. W. Cable, Phys. Rev. Lett. **24**, 16 (1970).
[16]W. Marshall and S. W. Lovesey, *Theory of Thermal Neutron Scattering* (Clarendon, Oxford, 1971).
[17]H. E. Nigh, S. Legvold, and F. H. Spedding, Phys. Rev. **132**, 1092 (1963).
[18]H. R. Child, Phys. Rev. B **18**, 1247 (1978).
[19]D. S. Ritchie and M. E. Fisher, Phys. Rev. B **5**, 2668 (1972).
[20]P. Lindgård, Phys. Rev. B **17**, 2348 (1978).